nature neuroscience

Pre-neuronal morphological processing of object location by individual whiskers

Knarik Bagdasarian[1,7], Marcin Szwed[2,7], Per Magne Knutsen[3,7], Dudi Deutsch[1,7], Dori Derdikman[4], Maciej Pietr[1,6], Erez Simony[5] & Ehud Ahissar[1]

In the vibrissal system, touch information is conveyed by a receptorless whisker hair to follicle mechanoreceptors, which then provide input to the brain. We examined whether any processing, that is, meaningful transformation, occurs in the whisker itself. Using high-speed videography and tracking the movements of whiskers in anesthetized and behaving rats, we found that whisker-related morphological phase planes, based on angular and curvature variables, can represent the coordinates of object position after contact in a reliable manner, consistent with theoretical predictions. By tracking exposed follicles, we found that the follicle-whisker junction is rigid, which enables direct readout of whisker morphological coding by mechanoreceptors. Finally, we found that our behaving rats pushed their whiskers against objects during localization in a way that induced meaningful morphological coding and, in parallel, improved their localization performance, which suggests a role for pre-neuronal morphological computation in active vibrissal touch.

In vertebrates, external signals usually do not make direct contacts with neuronal receptors. Instead, receptors are activated by signals that are first modified by mediating tissues. In the rodent vibrissae system, an extensively studied experimental model of active sensorimotor processing[1,2], the mechanoreceptors that sense vibrissal touch are located at the base of the whiskers, in the follicle-sinus complex[3]. The whisker hairs themselves are not innervated. Thus, processing of vibrissal touch is indirect, in the sense that the whisker acts as a mechanical transducer between the objects being touched and the mechanoreceptors of the follicle-sinus complex.

Recent studies on sensor-level encoding of natural-like or complex stimuli in vision and touch have shown that first-order neurons can perform complex computations. In the vibrissal somatosensory system, active sensor movements induce mechanical representations of object features[4–6] and render first-order neurons selective to active touch components: whisker motion, contact, detachment and vibration[7–11]. During active touch these neurons also encode object location in the azimuthal (front-back)[7] and radial (from the snout outward)[8] dimensions by firing time and rate, respectively[12,13]. How encodings of external features are implemented, and to what extent they depend on sensor embodiment, movement policies and closed-loop control is not yet known.

We observed that, in the vibrissal system, consistent with theoretical predictions[14–17], processing of object position already occurs at a pre-neuronal level. Using high-speed videography, automated whisker-tracking techniques[18], artificial whisking[7] in anesthetized rats, and self-generated whisking in head-fixed and freely moving rats, we found that, during active touch, the position of an object is reflected in kinematic and morphological variables. The morphological variables contain invariant representations of azimuthal and radial object location, which allows a fast and efficient determination of object position from whisker mechanics alone. These results are consistent with previous demonstrations of the importance of sensor morphology and embodiment in perception[5,19–22].

RESULTS

Artificial whisking

We induced artificial whisking in urethane-anesthetized rats by stimulating the facial motor nerve. Whisker trajectories in the horizontal plane (**Fig. 1**) were captured with a fast digital video camera (500 or 1,000 fps). Periods (2 s) of artificial whisking at 5 Hz were followed by rest periods (2 s) in blocks of 12 trains (trials). Whisking movement amplitudes in free air were 20.3 ± 5.2° (n = 39 rats).

Blocks of whisking in free air were interleaved with blocks of whisking against an object (a vertical pole) located at various azimuthal and radial distances from the whisker (**Fig. 1a**). In each trial, the object was placed at one of six points distributed across a triangular grid, which was scaled according to the length of the whisker (measured from its emergence from the skin surface to its tip, with an accuracy of 1 mm) and the amplitude of the movement. Along the radial dimension, the nodes of this grid were located at 30, 60 and 90% of the length of the whisker. The azimuthal positions were numbered 1 (posterior) to 3 (anterior). We focused on whisker angle (θ), angle protraction (θ_p, protraction after contact), angle absorption (θ_a, the amount of movement blocked by an object), global curvature ($G\kappa$, the maximal curvature along a spline fitted to the entire bending portion

[1]Department of Neurobiology, Weizmann Institute of Science, Rehovot, Israel. [2]Psychophysiology Laboratory, Institute of Psychology, Jagiellonian University, Kraków, Poland. [3]Department of Physics, University of California, San Diego, La Jolla, California, USA. [4]Rappaport Faculty of Medicine, Technion, Haifa, Israel. [5]Department of Psychology and the Neuroscience Institute, Princeton University, Princeton, New Jersey, USA. [6]Deceased. [7]These authors contributed equally to this work. Correspondence should be addressed to E.A. (ehud.ahissar@weizmann.ac.il).

Received 15 November 2012; accepted 11 March 2013; published online 7 April 2013; doi:10.1038/nn.3378

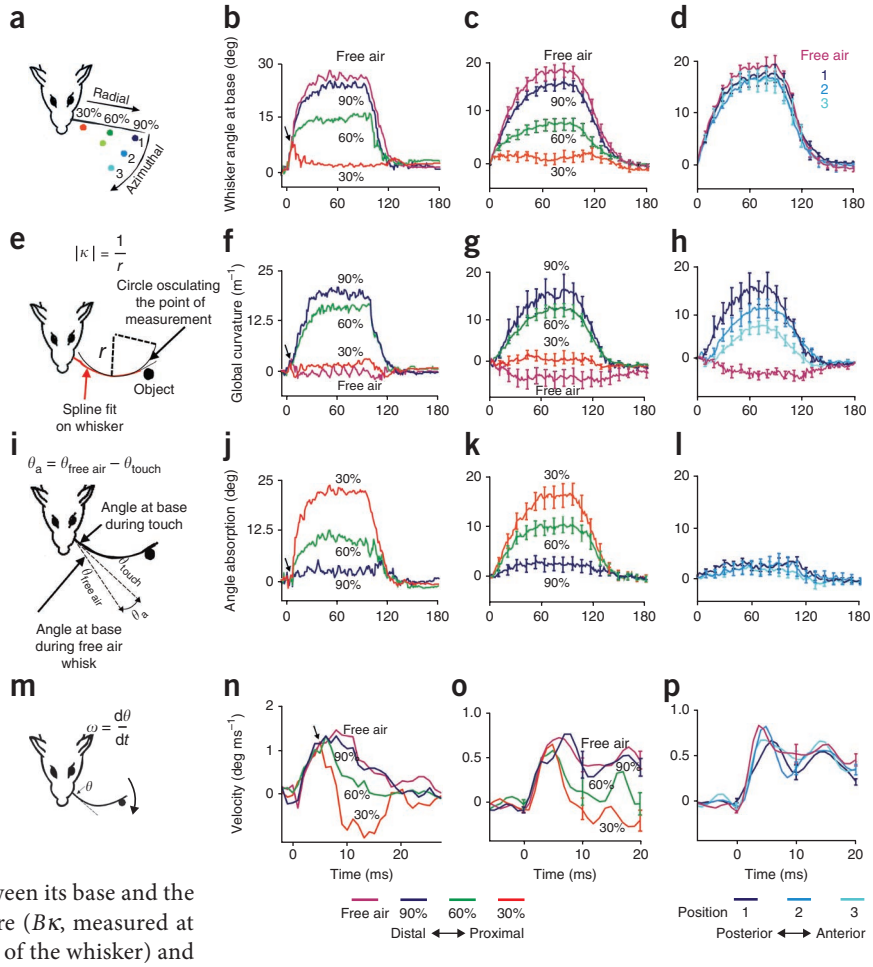

Figure 1 Effects of object position on morphological and kinematic variables in artificially whisking anesthetized rats. (**a**) Grid of pole positions. The curved arrow indicates the direction of whisker protraction. (**b**) The angular position of a single whisker during a single protraction and retraction cycle (whisk) in free air (magenta) and against an object located at the three radial positions (all at azimuthal position 1). The angle trajectory is shown unfiltered (1,000 Hz). (**c**) Data are presented as in **b**, but for the entire population of studied whiskers ($n = 27$ whiskers). (**d**) The angular position of the entire population of studied whiskers ($n = 31$ whiskers) during a single whisk in free air (magenta) and against an object located at the three azimuthal positions (all at a radial position of 90% of whisker length). (**e**) Schematic illustration of whisker curvature measurement. (**f**–**h**) Data are presented as in **b**–**d**, but for whisker global curvature. (**i**) Schematic illustration of whisker angle absorption measurement. (**j**–**l**) Data are presented as in **b**–**d**, but for whisker angle absorption. (**m**) Schematic illustration of whisker velocity measurement. (**n**–**p**) Data are presented as in **b**–**d**, but for whisker angular velocity (note the different time scales). Arrows in **b**, **f**, **j** and **n** denote contact onset. **b**, **f**, **j** and **n** were measured simultaneously at the same trial. $t = 0$ denotes the video frame before the first movement of the whisker was detected. Data are presented as mean ± s.e.m. Error bars are shown every 10 or 11 ms.

of the whisker, taken here to be the portion between its base and the point of contact with the object), base curvature ($B\kappa$, measured at the base of a spline fitted to a proximal segment of the whisker) and whisker angular velocity (ω). All of these variables can be read out either directly or indirectly at the follicle (see Discussion).

Radial and azimuthal coordinates

We first examined how whisker morphological and kinetic variables change when the object location varies only along the radial axis. In these experiments, the object was always positioned at the most posterior azimuthal position (position 1; **Fig. 1a**) and at the same angular distance from the resting whisker. A single trial example exhibited monotonic coding of the radial coordinate by θ, $G\kappa$, θ_a and ω (**Fig. 1**). The slight 83-Hz modulation of the angle visible in some of the trajectories is a result of the pulsating nature of the electrical nerve stimulation[7]. The rapid reduction of the whisker's angle (relative to the skin) after contact onset at 30% can be accounted for by a continuing protraction of the pad while the whisker is blocked by the object (see "Follicle-whisker interface" below).

This behavior of $G\kappa$, θ_a and ω was usually consistent across the population of whiskers studied here. We examined the mean trajectories of 27 whiskers using an automatic whisker tracker[18] (**Fig. 1**). From the mean trajectories, it was apparent that the global curvature monotonically decreased for more proximal object locations. Although this was typical behavior, it was not always true for individual whiskers. Following detailed tracking validation ($n = 6$ whiskers), a fully monotonic relationship was observed in two of the cases. Another two cases exhibited equal global curvature for radial distances of 60 and 90%, and the last two cases exhibited a larger global curvature for 60 than for 90%. Thus, although proximal touch at 30% of whisker length yielded the smallest global curvature in all cases, distal touch at distances ≥60% yielded variable, and not necessarily monotonic, global curvature. This is consistent with the variable, and sometimes non-monotonic, response ratios among individual neurons of the trigeminal ganglion to touch at radial locations of 60–90% (ref. 8).

We examined whisker trajectories from experiments in which the azimuthal position was varied from the most posterior (position 1; **Fig. 1a**) to the most anterior (position 3) while the radial position of the object was held constant at 90% of whisker length. Analysis of 31 whiskers revealed that the major effect of azimuthal object position was on $G\kappa$ (which decreased with more anterior positions), with θ_a and ω usually barely being affected (**Fig. 1**).

Quantitative population analysis

The significance of the effects described above was determined by quantifying the mean population behavior across all whiskers. Because stimulation conditions varied across experiments, which resulted in different movement amplitudes and velocities, $G\kappa$, θ_a and $\Delta\omega$ were normalized to allow comparison between whiskers (**Fig. 2**).

Radial object position was encoded by all three of these variables ($P < 0.001$, $F > 8$, ANOVA). The whisker bent extensively during distal touch, whereas it either did not curve at all or curved negatively during proximal touch (normalized mean of −0.24; **Fig. 2a**). Angle absorption was smaller during distal touch and larger during proximal touch (**Fig. 2b**). Whisker velocity was affected slightly by distal touch and strongly by proximal touch

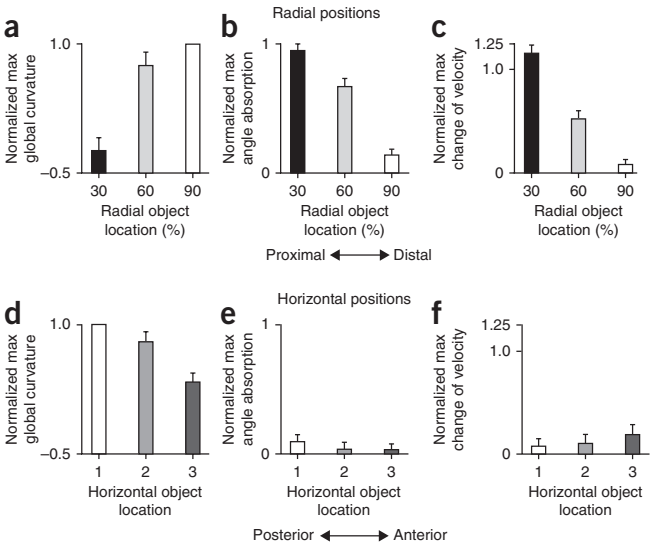

Figure 2 Mechanical encoding of object location by whiskers of artificially whisking anesthetized rats. (**a**–**c**) Encoding of the radial dimension by global curvature (**a**), angle absorption (**b**) and velocity changes (**c**) following touch ($n = 27$ whiskers). (**d**–**f**) Encoding of the azimuthal dimension by global curvature (**d**), angle absorption (**e**) and velocity changes (**f**) ($n = 31$ whiskers). Velocity changes were measured 10 ms after contact. All variables were normalized to allow inter-whisker comparisons. Curvature was normalized to maximum. Angle absorption and velocity changes were normalized relative to the free-air whisking (0 indicates no absorption or no deceleration, 1 indicates complete absorption or standstill; a value above 1 indicates a reversal in movement direction, such as that observed in the 30% trajectory in **Fig. 1n**). Peak values occurring during whisker protraction are depicted. Data are presented as mean ± s.e.m.

(**Fig. 2c**). In many cases of proximal touch, the direction of the movement of the whisker base changed as a result of the forward translation of the entire pad (**Fig. 1n**,**o**).

In contrast to the radial object position, azimuthal object position (at distal radial coordinates) was significantly encoded only by $G\kappa$. $G\kappa$ decreased as the object was contacted at more anterior positions ($P < 0.001$, $F > 8$, ANOVA; **Fig. 2d**). The θ_a and $\Delta\omega$ were essentially the same for the various azimuthal positions (θ_a, $P = 0.14$, $F = 2.0$; $\Delta\omega$, $P = 0.78$, $F = 0.25$; ANOVA; **Fig. 2e**,**f**).

Invariant representations in the $G\kappa$-θ_a phase plane

After analyzing each variable independently, we analyzed the angle absorption and global curvature variables concurrently (**Fig. 3**) for all six positions tested (**Fig. 1a**). The mean $G\kappa$ and θ_a were plotted as a function of time (**Fig. 3a**,**d**) and the two plots were combined into a common phase plane by collapsing their time axes (**Fig. 3b**). This resulted in a concurrent representation of object position, by $G\kappa$ and θ_a along a whisking cycle, being described by a trajectory in the phase plane of these two variables.

Throughout the entire contact duration, the mean ratio of $G\kappa$ to θ_a was invariant to changes in the azimuthal coordinate; at the radial coordinate of 90% whisker length (**Fig. 3b**), all of the azimuthal coordinates (positions 1, 2 and 3) yielded trajectories with the same slope, although of different magnitudes. The same occurred with the two azimuthal coordinates (positions 1 and 2) tested at the radial distance of 60%. Thus, a smaller slope (small $G\kappa$ and large θ_a) represents a smaller radial distance and a larger slope represents a large radial distance (**Fig. 3c**). The magnitudes of the trajectories in the phase plane were invariant to the radial coordinate and represented the azimuthal coordinate. All of the magnitudes measured at position 1 (posterior) were larger than those measured more anteriorly (**Fig. 3b**,**c**).

These data demonstrate the availability of a morphological coding scheme in which the ratio between $G\kappa$ and θ_a represents the radial distance (**Fig. 3e**) and their combined magnitude (vector length) represents the azimuthal angle of contact (**Fig. 3f**). Readout of these variables at any given moment after contact can provide the location of the object in the horizontal plane, after appropriate scaling by the relevant whisker motor variables.

Whisker angle and global curvature in freely moving behaving rats

We tested whether morphological coding can be generalized to natural whisking behavior by comparing morphological changes that occur during artificial whisking with those observed while freely moving rats performed an object localization task (**Fig. 4**). In brief,

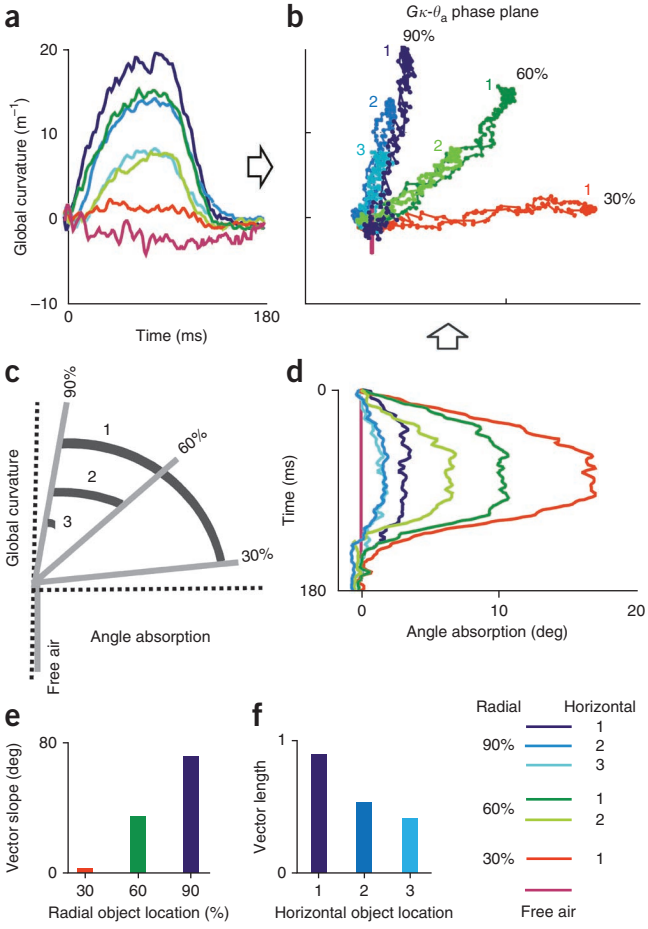

Figure 3 Morphological encoding in the $G\kappa$-θ_a phase plane. (**a**,**d**) Mean global curvature (**a**) and mean angle absorption (**d**) of the population of whiskers ($n = 19$) studied in all object positions in anesthetized rats. Collapsing the time dimension of **a** and **d** (arrows) yielded **b**. (**b**) Trajectories of whisker morphology in a $G\kappa$-θ_a phase plane; successive dots depict successive values of $G\kappa$ and θ_a during an average whisk at a resolution of 1 ms. (**c**) Phase plane invariants. Radial distances were coded by trajectory slopes, invariant to azimuthal positions, whereas azimuthal positions were coded by trajectory magnitudes, invariant to radial distances. (**e**,**f**) Representation of radial and azimuthal coordinates of object location by the slope (deg) and length of the phase-plane vector (arbitrary units), respectively.

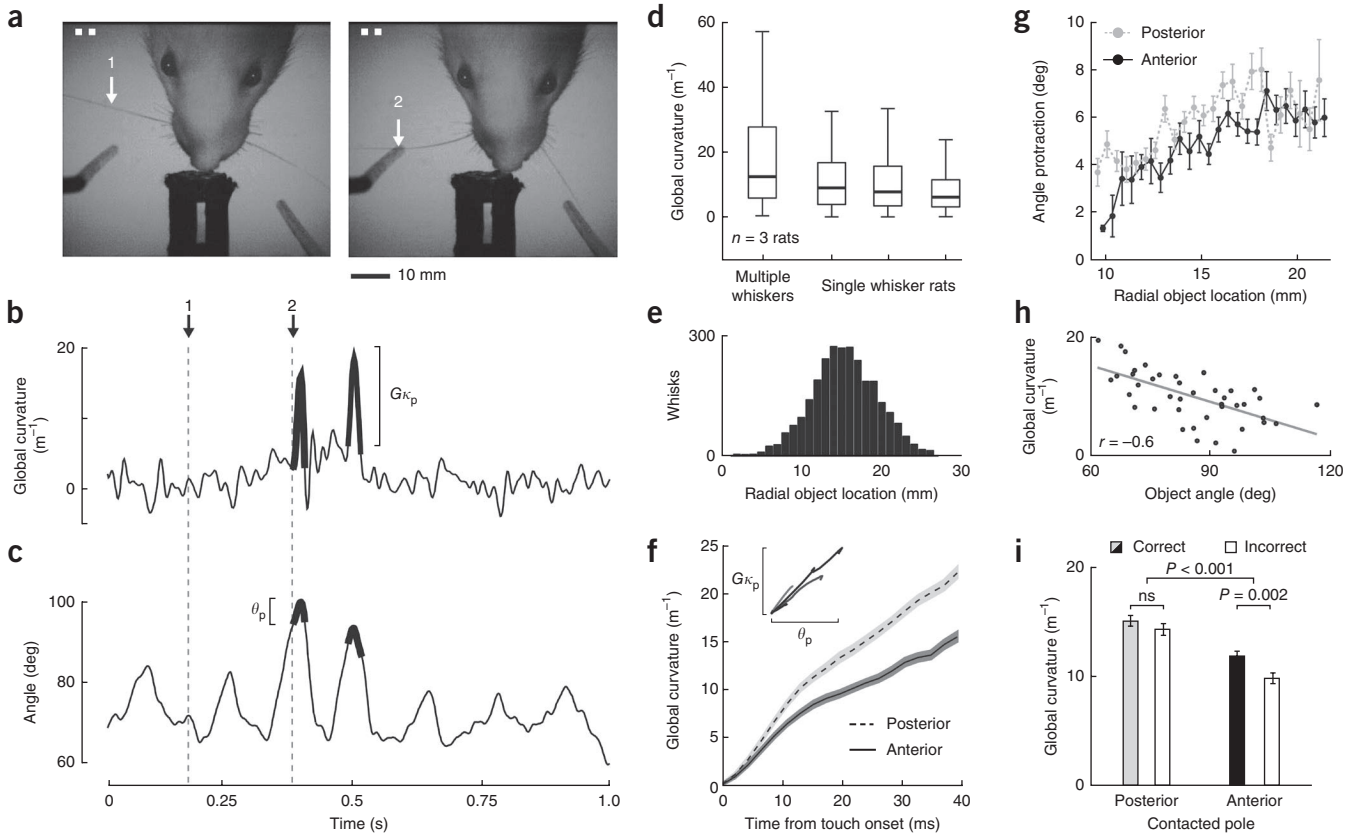

Figure 4 Angle and global curvature dynamics in freely moving rats during a localization task. (**a**) Two frames of a single-whisker rat performing the task[23]. White arrows indicate the tracked whisker in **b** and **c**. (**b**,**c**) $G\kappa$ and θ of the tracked whisker during a segment of the trial. Thick sections indicate periods when the whisker contacted the pole. (**d**) Population summary of $G\kappa_p$ (see **b**) (box plots: medians, quartiles and ranges). Rats with all whiskers intact are grouped together ($n = 109$ whisks) and three rats that performed the task with a single whisker (C2) are shown individually ($n = 882$, 1,043 and 1,099 whisks). (**e**) Distribution of the radial location of touch during localization ($n = 3$ single-whisker rats); bin size is 1 mm. (**f**) $G\kappa_p$ (mean ± s.e.m.) versus time from onset of contact with either the posterior (dashed, light gray) or anterior (solid, dark gray) object. Inset shows four individual whisks; θ_p scale = 0–15°, $G\kappa_p$ scale = 0–30 m^{-1}. (**g**) θ_p as a function of radial object location, from the onset of contact. θ_p values were grouped (bin size = 0.5 mm) and then averaged (mean ± s.e.m.). (**h**) Correlation between $G\kappa_p$ (log scale) and object angle in individual contacts ($n = 43$ contacts) of a single localization session. The solid gray line is the least square linear fit ($r = -0.6$, $P < 0.001$). (**i**) Mean (± s.e.m.) $G\kappa_p$ in correct (solid) and incorrect (empty) trials. Sample size was three rats and 1,657 and 1,072 whisks for posterior and anterior contacts, respectively, in **f**, **g** and **i**.

our rats were required to report the relative position of two vertical poles, positioned to the sides of a nose-poke detector at a variable anterior-posterior offset (<20 mm; **Fig. 4a**). Whisking behavior and object palpation during object localization involved whisk amplitudes that ranged between a few degrees to a few tens of degrees and frequencies in the 5–20-Hz range. These rats were capable of hyper-accurate azimuthal localization with all or a reduced set of intact whiskers[23].

Increases in whisker curvature following contact were frequently observed while rats, with either a single whisker intact on either side of the snout ($n = 3$ rats; **Supplementary Movie 1**) or with multiple whiskers intact ($n = 3$ rats; **Supplementary Movie 2**), palpated an object during localization, as the rats continued to protract their whiskers after object contact was initially made (**Fig. 4c**). The change in $G\kappa$ in each whisk cycle was computed as the maximal $G\kappa$ during contact minus $G\kappa$ in the last frame before contact ($G\kappa_p$; **Fig. 4b**). The rats exhibited a large range of curvature changes (**Fig. 4d**), comparable in magnitude to those displayed during artificial whisking. The rats contacted the object at a wide range of radial locations, but typically within 40–70% of the whisker length (16.4 ± 0.08 mm from base, mean ± s.e.m.; **Fig. 4e**). When an object was contacted, the duration of contact was greater than 30 ms in more than 50% of contact events (data not shown). During contact, $G\kappa$ developed such that, starting at 10 ms after contact, it conveyed information about the azimuthal coordinate of object position ($P < 0.025$, Kolmogorov-Smirnov test; **Fig. 4f**)[24].

Although θ_a can be sensed at the follicle through tension developed between the intended and actual movement, it cannot be measured by an external observer when whisking is self-generated. We therefore analyzed a complementary variable in self-generated whisking, angle protraction. Following previous studies[15,16] we defined angle protraction (θ_p) as the angle of further protraction after touch onset (**Fig. 4c**). Angle protraction is identical to the 'theta push' described in refs. 15,16, and was similarly defined to equal 0° at the angle at which the vibrissa first makes contact with the object. When the motor command to the follicle is constant, θ_p and θ_a are completely complementary: their sum equals the intended protraction. With the light-touch strategy exhibited by our rats[12], θ_p decreased with decreased radial distance (**Fig. 4g**), suggesting that protraction was increasingly blocked by increased counter torque induced by the object[14,16].

Furthermore, we found that, in individual object localization sessions, the maximal $G\kappa$ encountered during touch was inversely related to the azimuthal object location, as represented by the angle of the

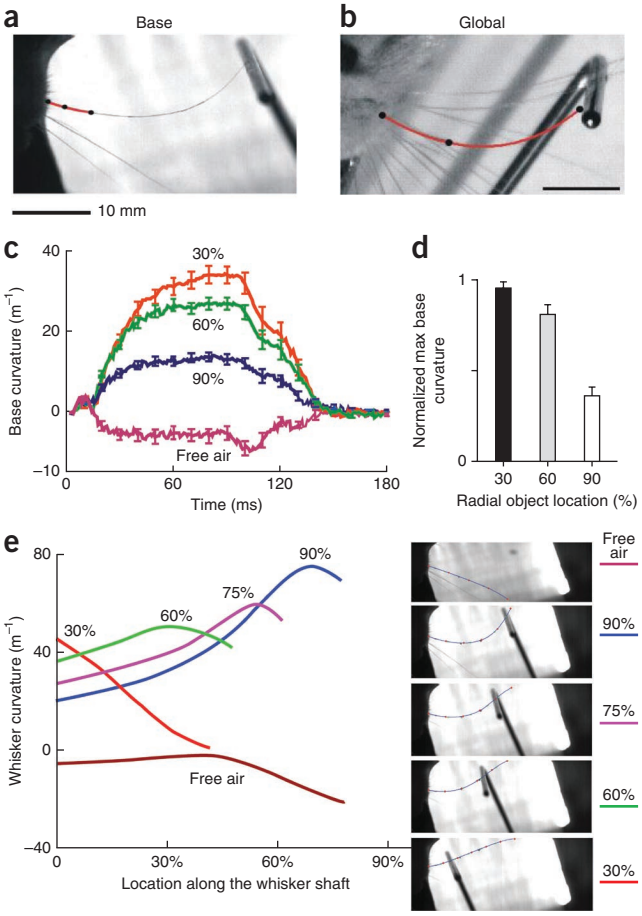

Figure 5 Curvature at the whisker base and along the whisker shaft in anesthetized rats. (**a**,**b**) Three-point spline fits (red) for the base (**a**) and global (**b**) measurements (maximum protraction, 90% radial distance). Scale bar denotes 10 mm. (**c**) Whisker base curvatures for three radial object positions (mean ± s.e.m. for 17 whiskers). (**d**) Normalized maximal values of whisker base curvature for the same whiskers. (**e**) Analysis, as a function of radial object position, of single-whisker curvature along the whisker shaft in the frame corresponding to the time of maximum protraction (frames are shown to the right). Curvature is depicted as a function of the point along the whisker at which it was locally computed.

object relative to the head (**Fig. 4h**), consistent with artificial whisking (**Fig. 2d**). Nevertheless, whether morphological coding was used by these rats could not be determined, as the phase-plane's vector length (**Fig. 3f**) cannot be computed without knowing the motor variables that determine θ_a. Still, our data suggest that morphological variables do affect performance in this task. Global curvature during contacts with the anterior object was significantly larger during correct (11.9 ± 0.39 m^{-1}) than incorrect trials (9.8 ± 0.48 m^{-1}, mean ± s.e.m.; $P = 0.002$, Kolmogorov-Smirnov test; **Fig. 4i**).

Curvature at the base of and along the whisker

The whisker is tapered and thickest at its base. Thus, the mechanical properties of the whisker shaft vary along its length. To study mechanical effects along the whisker shaft, we performed additional experiments at a higher imaging resolution (~40 µm per pixel, see Online Methods). This facilitated measurements of the whisker base and examination of how a contact position is encoded by base morphology, rather than global morphology (**Fig. 5a**,**b**). In general, $B\kappa$ decreased with increasing radial distance ($P < 0.001$, $F > 8$, ANOVA, $n = 17$ whiskers; **Fig. 5c**,**d**), as predicted by theoretical derivations[14,16].

This coding of radial distance by $B\kappa$ was the inverse of that exhibited by $G\kappa$ (**Figs. 1g** and **2a**). This suggests that the local curvature is not constant, but instead changes along the whisker during contact. We measured curvature along the whisker shaft when the whisker was maximally protracted ($n = 3$ whiskers from 2 rats; **Fig. 5e** and Online Methods). For the most proximal contact location (30% of whisker length), the whisker shaft increasingly curved toward the base. During contact between 60 and 90% of whisker length, local curvature peaked somewhere between the base and contact location of the whisker. As a result, $B\kappa$ was largest during proximal touch (30%), whereas $G\kappa$ was largest for distal touch (90%), consistent with theoretical predictions based on elastic beam theory[14,15].

Whisker angle and base curvature in head-fixed awake rats

Whether morphological coding by $B\kappa$ generalizes to self-evoked whisking was tested by comparing $B\kappa$ changes occurring during artificial whisking in anesthetized rats with those observed while awake, head-fixed rats whisked against similar pole objects. Whisking amplitudes in head-fixed rats ($n = 7$ rats) ranged between a few degrees to a few tens of degrees and frequencies ranged between 5–15 Hz. Contacts with the object (**Fig. 6a** and **Supplementary Movie 3**) often resulted in robust increases in $B\kappa$ ($B\kappa_p$; **Fig. 6b**), as the rats continued to protract the whiskers after contact.

Curvature changes in head-fixed rats were on the same order of magnitude as those measured during artificial whisking (**Figs. 5** and **6**) and their dependency on the radial distance showed a similar trend as in artificial whisking: $B\kappa$ decreased with increasing radial distance ($P < 0.001$, $F > 8$, ANOVA; **Fig. 6d**). The representation of the radial distance by $B\kappa$ was already evident a few milliseconds after contact, and developed further during the following few tens of milliseconds (**Fig. 6e**), with dynamics that probably reflect a rapid feedback mechanism[25].

Reliability of phase plane representations

The morphological variables that we measured are inter-related: θ_p and θ_a sum to the intended angle, and $B\kappa$ and $G\kappa$ are inter-related for a given whisker and radial distance of contact (**Fig. 5e**). θ_a is also inversely related to the base curvature: the stronger the blocking of the whisker, the smaller the $B\kappa$ that will develop[14]. We examined the reliability of morphological coding in the phase plane defined by θ_p, which can be measured in awake animals, and $B\kappa$, which is proportional to the moment at the base and thus contains receptor-relevant information. In this phase plane, the slopes of the trajectories decreased with the radial distance of contact[14,16] (**Fig. 7a**).

We examined the reliability of morphological coding and its ability to follow, and possibly underlie, fast behavioral feedback[25,26] in single contacts using high-resolution tracking. The low variability of artificial whisking trajectories (single-whisk amplitudes deviated by ±2.2% from the mean whisk amplitude of 37.3°, $n = 27$ whisks) allowed us to determine that, in principle, the combination of $B\kappa$ and θ_p can encode contact location reliably as early as 15 ms after contact onset (**Fig. 7b**). Trajectories displayed by the whiskers of head-fixed awake rats during object contact covered a similar range of orientations and magnitudes as those in artificially whisking anesthetized rats (**Fig. 7c**) while, as expected, displaying higher variability. Despite this higher variability, coarse discrimination of the radial distance of contact was possible in single trials (**Fig. 7d**). During self-whisking, it is expected that reproducibility is maintained in motor-sensory contingencies[27] rather than in sensory or motor variables alone. If this is the case, morphological processing during self-evoked whisking should involve tight motor-sensory control.

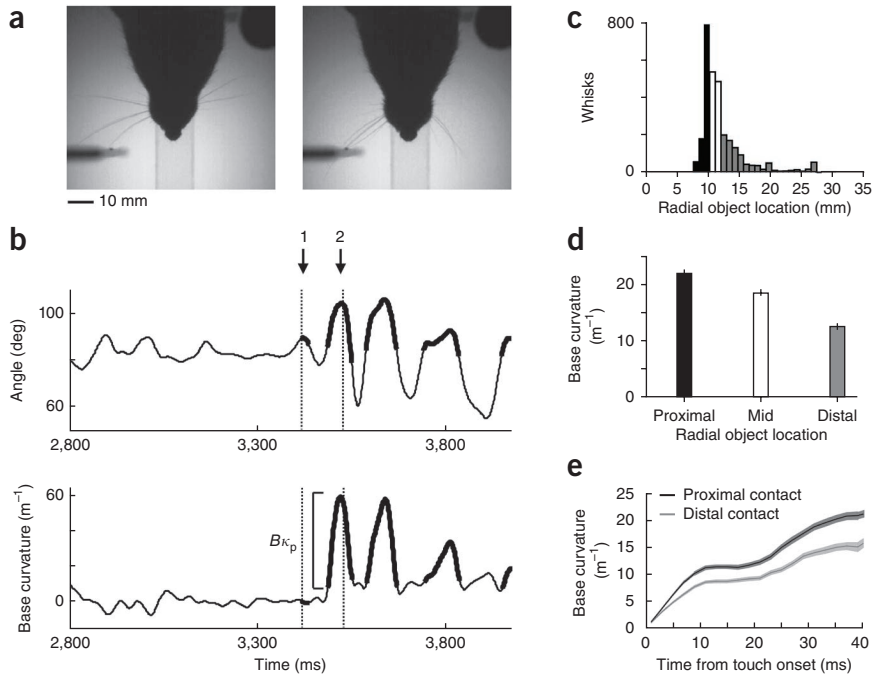

Figure 6 Angle and base curvature dynamics in awake, head-fixed rats. An example of a trial in which a head-fixed rat whisked against an object and contacted it 17 times (first five are shown as bold sections in **b**) is shown. Time measured from trial onset. (**a**) Frame 1 was taken at the onset of the first touch in the trial, and frame 2 was taken at maximum curvature of the next touch (**Supplementary Movie 3**). (**b**) Whisker base angle (top) and base curvature (bottom) traces. Thick sections mark video-verified contacts. Curvature is presented relative to the value at the onset of the first contact in the trial. (**c**) The distribution of radial object position on contact (R), defined as the distance (in millimeters) between whisker base and whisker pole contact at the time of touch onset in a given whisk cycle ($n = 3{,}011$ contacts). The population was divided into three equally sized groups: R ≤ R1 (proximal), R1 < R ≤ R2 (mid) and R > R2 (distal) (R1 = 10.1 mm, R2 = 11.9 mm); each group contained 1,003 or 1,004 whisking cycles. (**d**) The difference between the maximum value of base curvature following touch and the value at touch onset ($B\kappa_p$) is depicted as a function of radial object position. Data are presented as mean ± s.e.m. for 664 random samples from each of the groups defined in **c**. (**e**) Change in base curvature (mean ± s.e.m.) as a function of time from contact onset for the proximal and distal groups of R. Bin size is 2 ms.

Follicle-whisker interface

The larger θ_a at more proximal radial contact locations (**Figs. 1–3**) could reflect one of the following scenarios. The whisker might bend close to the base, near the mouth of the follicle, while the intrinsic muscles of the follicle would continue to move the follicle unperturbed (a hinge-like joint). Alternatively, whisker and follicle might form a rigid joint. These scenarios would result in different distributions of forces in the follicle, and therefore different patterns of mechanoreceptor activation.

To distinguish between these two scenarios of angle absorption, we repeated the artificial whisking procedure during placement of the object at different radial locations while one-third of the upper part of one or two whisker follicles was surgically exposed (Online Methods). During this surgery, the integrity of exposed follicles and intrinsic muscles was carefully maintained. The moving, exposed follicles were recorded with a high-speed camera fitted with a high-magnification lens. The resulting whisking amplitudes were similar to those obtained during artificial whisking with tissue around the follicles completely intact ($P = 0.13$, t test).

We examined the movements of exposed follicles during whisking in free air and against objects at the 30, 60 and 90% radial positions (**Fig. 8a** and **Supplementary Movie 4**). The relative angles of the whisker and exposed follicle were analyzed by plotting (using the camera lucida technique) the alignment of the follicle during movement, using structure-from-motion cues in the movie for outlining of the follicle (**Fig. 8a**,**b**).

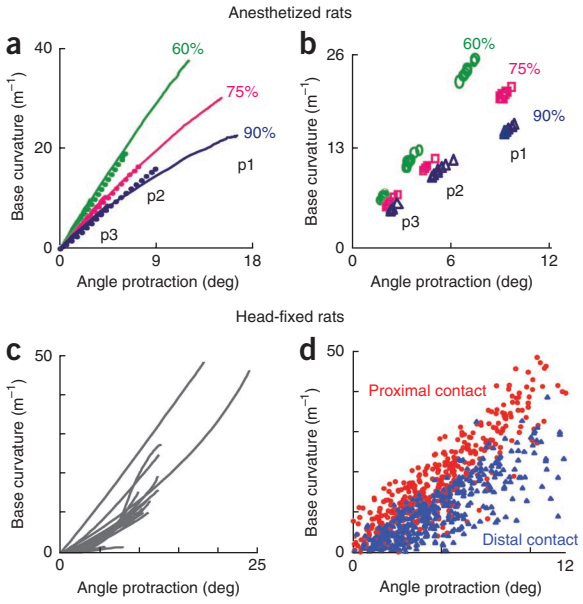

Figure 7 Single-cycle, single-whisker morphological encoding in the $B\kappa$-θ_p phase plane. In all panels, the change in base curvature from baseline ($B\kappa_p$) is depicted. (**a**) Single-cycle encoding in an artificially whisking anesthetized rat. Trajectories of whisker morphology during a single protraction epoch (from contact onset to peak protraction) recorded at a resolution of 1 ms. Azimuthal positions are from posterior (p1, thin line), through intermediate (p2, dotted line) to anterior (p3, thickest line), and radial positions are denoted by percent of whisker length. (**b**) Reproducibility of single-cycle encoding in an anesthetized rat. The phase-plane values are for the same whisker as in **a**, and are depicted for eight trials (per condition), 15 ms after touch onset (one data point per whisk cycle). (**c**) Single-cycle trajectories (from contact onset to peak protraction) in one trial of a head-fixed awake rat recorded at a resolution of 2 ms; 16 protraction epochs are shown. (**d**) Single-cycle encoding in a head-fixed awake rat (whisker C2), sorted by the radial distance of contact (**Fig. 6c**) and measured 16 ms after touch onset (one data point per whisk cycle, $n = 664$ cycles in each group data pulled from all seven rats).

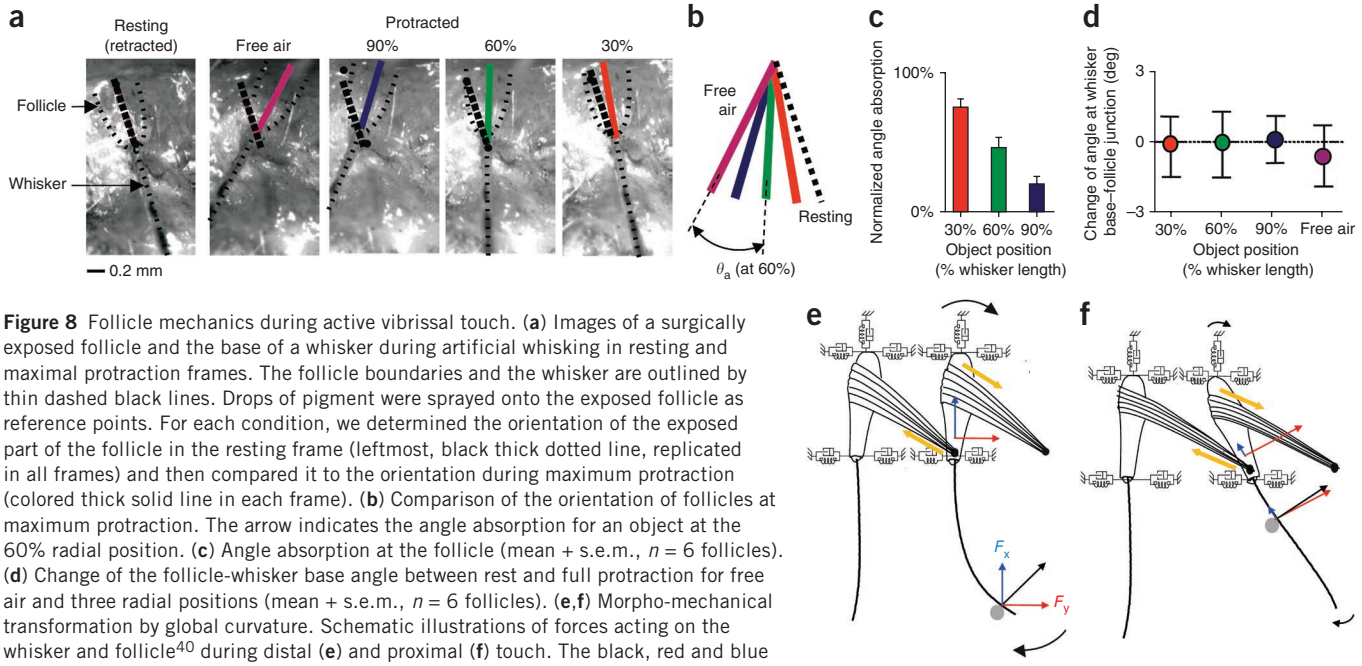

Figure 8 Follicle mechanics during active vibrissal touch. (**a**) Images of a surgically exposed follicle and the base of a whisker during artificial whisking in resting and maximal protraction frames. The follicle boundaries and the whisker are outlined by thin dashed black lines. Drops of pigment were sprayed onto the exposed follicle as reference points. For each condition, we determined the orientation of the exposed part of the follicle in the resting frame (leftmost, black thick dotted line, replicated in all frames) and then compared it to the orientation during maximum protraction (colored thick solid line in each frame). (**b**) Comparison of the orientation of follicles at maximum protraction. The arrow indicates the angle absorption for an object at the 60% radial position. (**c**) Angle absorption at the follicle (mean + s.e.m., $n = 6$ follicles). (**d**) Change of the follicle-whisker base angle between rest and full protraction for free air and three radial positions (mean + s.e.m., $n = 6$ follicles). (**e**,**f**) Morpho-mechanical transformation by global curvature. Schematic illustrations of forces acting on the whisker and follicle[40] during distal (**e**) and proximal (**f**) touch. The black, red and blue straight arrows represent the equivalent and components of the reaction force induced by the object. The yellow arrows represent muscle contractions. The curved black arrows represent follicle and whisker azimuthal rotations.

In all of the exposed follicle experiments, angle absorption also occurred at the level of the follicle ($n = 6$; **Fig. 8c**). The difference between θ_a of the follicle and that of the whisker base was negligible ($n = 6$ follicles, $P = 0.94$, $F = 0.13$, ANOVA; **Fig. 8d**). Thus, the follicle-whisker junction remained rigid during movement, even during whisking against an object located in the most proximal (30%) radial position.

DISCUSSION

In the rat vibrissal system, mechanoreceptors situated in the whisker follicle transduce signals that are initially processed mechanically by the external shaft of the whisker. We found that, consistent with theoretical predictions, the mechanical responses of the whisker shaft contained morphological and dynamic representations of object location during active touch. The radial and azimuthal coordinates of the position of the contacted object were reliably represented in phase planes spanned by pairs of morphological variables of the whisker. Measurements in head-fixed and freely moving behaving rats revealed that rats apply forces that allow meaningful morphological coding, that coding is reliable as fast as 15 ms after contact and that localization accuracy in behaving rats is correlated with code availability. Our results do not show how these codes are read out, but indicate that mechanical transformation from the whisker to the follicle is rigid and suggest possible readout mechanisms, consistent with previous suggestions.

Morphological phase planes

Consistent with theoretical predictions emerging from elastic beam theory[14,16,28], we found that, during active touch, the $B\kappa$ of a whisker was inversely related to the radial distance of contact (**Figs. 5–7**). In contrast, $G\kappa$, evaluated here as the maximal curvature along the whisker, generally increased with radial distance (**Figs. 1–5**). Our results further demonstrate that $G\kappa$ and θ_a display complementary representations. Given that the follicle and follicle-whisker junction are rigid (**Fig. 8**) and muscle force typically does not overcome the resistance of stationary objects (**Fig. 4g**), θ_a increased and $G\kappa$ decreased with decreased radial distance (**Figs. 1–3**). In fact, the combination of θ_a and $G\kappa$ encodes not only radial distance, but also any location in the horizontal plane (spanned by the azimuthal and radial coordinates), as both are affected in a complementary fashion by the azimuthal coordinate of the object. These dependencies can be mapped onto the $G\kappa$-θ_a phase plane, such that the slope of the trajectory encodes radial distance and the magnitude of the trajectory in the phase plane (vector length) encodes azimuthal angle (**Fig. 3**).

Meaningful phase planes can be composed from any pair of morphological variables (**Fig. 7**). Of these phase planes, all accessible to the brain of the rat, only those based on θ_p are directly accessible to an external observer when whisking is controlled by the rat. Thus, θ_p-based phase planes are useful when analyzing active touch in awake rodents.

Efficient morphological coding

An important aspect for downstream processing, demonstrated here in the $B\kappa$-θ_p phase plane, is that the variables of the phase plane were already valid by 15 ms after object contact (**Fig. 7**; coarse position information was available even earlier; **Figs. 4f** and **6e**), which allows rapid decoding of radial distance even before the most rapid motor reaction can take place[25,26]. In fact, studies on encoding by first-order neurons of the trigeminal ganglion have shown that, during contact, most information about radial object position is exhibited in the first 20 ms of the firing following touch[8]. This indicates that reading out whisker mechanical codes[14,15] is also rapid. Thus, reducing whisking cycle time, such as during palpation, does not necessarily interfere with morphological coding.

In our experiments with anesthetized rats, radial distance was reliably encoded by θ_a alone; the shorter the distance, the stronger the blocking of whisker protraction (**Fig. 4g**) and the larger the θ_a

(**Fig. 2b**). However, the readout of such coding would not be invariant to changes in whisking amplitude or, more accurately, to changes in the magnitude of the motor command, and would therefore be ambiguous. For example, θ_a would be similar for a given muscle activation against near objects and for a weaker muscle activation against more distal objects. In contrast, the ratio between $G\kappa$ and θ_a, or between $B\kappa$ and θ_p, if read out correctly, can provide radial coding that is invariant to whisking amplitude, as indicated by these ratios being constant during the entire course of protraction (after contact) for a given radial distance (**Figs. 3** and **7**).

Implications for active touch

Pre-neuronal processing, that is the generation of specific representations of the environment before neuronal processing, should be carefully controlled during active touch to optimize perception. In awake, self-whisking rats, morphological encoding exhibits large variations (**Figs. 4**, **6** and **7**) as a result of variations in motor variables, such as whisker set-point, amplitude, velocity and applied force. Reading of the morphological code must therefore be scaled by the brain accordingly. Scaling signals can be provided by proprioceptive-like mechanoreceptors[7,12], internal models based on efference copies[29] or both[30]. The exact use of morphological cues must be continuously calibrated in the brain[31–33] as a result of continuous changes in whisker morphology[21] and must be scaled to the actual motor outputs applied during an actual palpation epoch. These constraints suggest that morphological cues are used most efficiently in closed-loop perceptual processing loops[34].

Coordinates of radial and azimuthal object position are not encoded by morphological variables alone. Radial position is also encoded by the decrease in whisker velocity (**Figs. 1n**,**o** and **2c**), and azimuthal position by contact time[7]. As both these codes are transient, they are only valid around the time of contact. In contrast, the morphological variables yield useful information throughout contact duration. During active touch, a rat may favor one code over another by selecting different motor strategies. For example, when using extremely light touch[26], contact time will reliably represent azimuthal object position, whereas whisker morphology will not[2,12,35]. In contrast, when application of muscle force continues after contact has been made, whisker morphology will provide a continuous and reliable measure of object position in the radial and azimuthal directions. Notably, rats appear to exploit both temporal and morphological cues in some conditions, in a sequential order, for azimuthal localization[36].

Mechanical readout

Interactions between the whisker, its follicle and the associated intrinsic muscle do not occur at a single point, but rather along a few millimeters of the follicle length, which contains mechanoreceptors of several types and spatial orientations[3]. It is not yet clear whether the length of the follicle can be regarded as a linear extension of one canonical interaction point[37,38] or if substantial coding occurs along the follicle such that the axial coordinate of a receptor is a coding variable. The specific mapping between mechanical variables of the external shaft and torques and forces in the follicle is also not yet known. The nature of this mapping depends crucially on the rigidity of the follicle's collagenous capsule. With a rigid capsule, the mapping would depend only on the moments and forces at the base of the whisker (as a result of the rigid connection between the whisker and the follicle; **Fig. 8**)[15,16]. However, if the follicle's capsule does convey stresses from the surrounding tissue to its internal mechanoreceptors, then all muscle- and tissue-related degrees of freedom[39–41] should be taken into account.

Theoretical considerations suggest that if the whisker and its interactions are confined to one plane, most of the mechanical stresses applied to the external shaft of the whisker can be extracted by reading out the moment and the axial force at the base[15]. As the axial force has indeed been shown to affect neuronal responses substantially[42], the following scheme (**Fig. 8e**,**f**) appears valid for mechanical readout of morphological coding of the whisker shaft. This scheme suggests that changes in $G\kappa$ and θ_a result in orthogonal changes of forces in the follicle. Contact with an object that generates a global curvature (**Fig. 8e**), such that the tangent to the whisker at the contact point is at a substantial angle to the long axis of the follicle, yields a reaction force whose components along the axial (F_x, force parallel to the long axis of the follicle) and transverse (F_y, force perpendicular to the long axis) axes of the follicle are both substantial. In contrast, a contact that does not generate a substantial global curvature (as is the case with proximal contact; **Fig. 8f**) yields a reaction force mostly in the transverse direction. This model is consistent with a recent suggestion based on curvature measurements in head-fixed behaving mice[43]. This scheme assigns complementary coding information to base and global curvatures, representing moment at the base and whisker angle at the point of contact, respectively.

The rigid follicle-whisker junction (**Fig. 8a–d** and **Supplementary Movie 4**) ensures the preservation of the coding expressed by the two orthogonal force components (F_x and F_y) in the follicle. Of these two components, F_x is probably more informative, as F_y is likely overridden by the moment at the base[15,16,43]. A separation of the readout of the orthogonal force components (F_x and the base moment), possibly through an orthogonal alignment of sets of spine, lanceolate and small-caliber endings at the follicle[3], could provide an immediate mechanical readout mechanism. Such a mechanism may be more sensitive at the deep part of the follicle because of larger spring constants of the tissue[40].

Methodological and theoretical issues

The magnitudes of angular and curvature morphological variables was similar across anesthetized, head-fixed and freely moving behaving rats (**Fig. 1–6**; also see refs. 24,44). Still, as whisking data from behaving rats are highly variable and are not readily controlled by the experimenter, revelation of the principles of morphological encoding in this system would not be possible without the use of systematic studies in anesthetized rats and high-resolution video recording (~40 μm per pixel).

The top-down viewpoint used during high-speed video recordings and whisker tracking does not directly capture vertical and torsional excursions of whisker trajectories. Although torsional excursions likely added noise to our measurements, vertical excursions likely did not, given their small amplitudes[45].

Morphological processing by whisker is an excellent example in which theory and experiments can iterate successfully. The detailed derivations of the theory of elastic beams and its application to whisker mechanics[14–16,28] (D. Golomb, A. Hires & K. Svoboda, *Soc. Neurosci. Abstr.* **677.03**, 2012) was instrumental in guiding our experiments and interpreting the results. We believe that a comprehensive understanding of morphological processing in particular, and vibrissal sensing in general, is not possible without tight iterative interactions between theory and experiments.

Pre-neuronal morphological computation

Pre-neuronal transformations occur in every sensory organ. For example, acoustic inputs are transformed by bones in the middle

ear, optical signals are transformed by the cornea and eye fluids, and tactile inputs are transformed by the skin. Some of these transformations appear to be more passive in nature, whereas others appear to take part in active sensing. In the vibrissal system, pre-neuronal morphological transformations appear to be components of active touch, along with motor, physical, mechanical and neuronal transformations; it is suggested that, in the active-touch loop, morphological variables translate the interaction of motor variables with external physical variables to within-follicle mechanical variables (**Supplementary Fig. 1**).

The relatively large pre-neuronal morphological space of the whisker[1,4,5,7,8,11,14,16,18,23,46] and the apparent redundancy in follicle processing[3,14,16,37] permit substantial flexibility in vibrissal mechanical processing. Furthermore, the detailed control of whisker dynamics by motor circuits[29,41,47–50] allows dynamic control of this mechanical processing during sensory acquisition. We propose that these motor-controlled pre-neuronal computations are an integral processing component of vibrissal motor-sensory loops.

METHODS

Methods and any associated references are available in the online version of the paper.

Note: Supplementary information is available in the online version of the paper.

ACKNOWLEDGMENTS

We thank D. Goldian and S. Haidarliu for technical assistance, N. Rubin for programming, B. Schick for reviewing, M. Hartmann and J. Solomon for critically reading the manuscript and for extensive and helpful discussions, and C. Moore, J. Ritt, L. Gomez, S. Barash and G. Bi for helpful suggestions. The article is dedicated to our late friend and colleague Maciej Pietr for his significant contribution to this work. This work was supported by the Israel Science Foundation (grant 749/10), the Minerva Foundation funded by the Federal German Ministry for Education and Research, the United States–Israel Binational Science Foundation (grant 2011432), the Ministry of Science and Technology (Israel), the Ministry of Research (Taiwan), and the Chief Scientist, Israeli Ministry of Health. K.B. acknowledges support by the KAMEA program administered by the Ministry of Absorption (Israel). P.M.K. was supported by a Long-Term Fellowship from the Human Frontier Science Program. E.A. holds the Helen Diller Family Professorial Chair of Neurobiology.

AUTHOR CONTRIBUTIONS

K.B. and M.S. performed the artificial whisking experiments. K.B. designed and K.B. and M.S. performed the exposed follicle experiments. P.M.K., D. Deutsch and M.P. performed the head-fixed and freely moving experiments. K.B., M.S., P.M.K., D. Deutsch, D. Derdikman and E.S. analyzed data. K.B., M.S., P.M.K., D. Deutsch, D. Derdikman, E.S. and E.A. prepared figures. K.B., M.S., P.M.K., D. Deutsch, D. Derdikman and E.A. wrote the manuscript.

COMPETING FINANCIAL INTERESTS

The authors declare no competing financial interests.

1. Kleinfeld, D., Ahissar, E. & Diamond, M.E. Active sensation: insights from the rodent vibrissa sensorimotor system. *Curr. Opin. Neurobiol.* **16**, 435–444 (2006).
2. Diamond, M.E., von Heimendahl, M., Knutsen, P.M., Kleinfeld, D. & Ahissar, E. 'Where' and 'what' in the whisker sensorimotor system. *Nat. Rev. Neurosci.* **9**, 601–612 (2008).
3. Ebara, S., Kumamoto, K., Matsuura, T., Mazurkiewicz, J.E. & Rice, F.L. Similarities and differences in the innervation of mystacial vibrissal follicle-sinus complexes in the rat and cat: a confocal microscopic study. *J. Comp. Neurol.* **449**, 103–119 (2002).
4. Hartmann, M.J., Johnson, N.J., Towal, R.B. & Assad, C. Mechanical characteristics of rat vibrissae: resonant frequencies and damping in isolated whiskers and in the awake behaving animal. *J. Neurosci.* **23**, 6510–6519 (2003).
5. Ritt, J.T., Andermann, M.L. & Moore, C.I. Embodied information processing: vibrissa mechanics and texture features shape micromotions in actively sensing rats. *Neuron* **57**, 599–613 (2008).
6. Wolfe, J. *et al.* Texture coding in the rat whisker system: slip-stick versus differential resonance. *PLoS Biol.* **6**, e215 (2008).
7. Szwed, M., Bagdasarian, K. & Ahissar, E. Encoding of vibrissal active touch. *Neuron* **40**, 621–630 (2003).
8. Szwed, M. *et al.* Responses of trigeminal ganglion neurons to the radial distance of contact during active vibrissal touch. *J. Neurophysiol.* **95**, 791–802 (2006).
9. Lottem, E. & Azouz, R. Dynamic translation of surface coarseness into whisker vibrations. *J. Neurophysiol.* **100**, 2852–2865 (2008).
10. Arabzadeh, E., Zorzin, E. & Diamond, M.E. Neuronal encoding of texture in the whisker sensory pathway. *PLoS Biol.* **3**, e17 (2005).
11. Andermann, M.L., Ritt, J., Neimark, M.A. & Moore, C.I. Neural correlates of vibrissa resonance; band-pass and somatotopic representation of high-frequency stimuli. *Neuron* **42**, 451–463 (2004).
12. Knutsen, P.M. & Ahissar, E. Orthogonal coding of object location. *Trends Neurosci.* **32**, 101–109 (2009).
13. Kleinfeld, D. & Deschênes, M. Neuronal basis for object location in the vibrissa scanning sensorimotor system. *Neuron* **72**, 455–468 (2011).
14. Birdwell, J.A. *et al.* Biomechanical models for radial distance detection by rat vibrissae. *J. Neurophysiol.* **98**, 2439–2455 (2007).
15. Quist, B.W. & Hartmann, M.J. Mechanical signals at the base of a rat vibrissa: the effect of intrinsic vibrissa curvature and implications for tactile exploration. *J. Neurophysiol.* **107**, 2298–2312 (2012).
16. Solomon, J.H. & Hartmann, M.J. Radial distance determination in the rat vibrissal system and the effects of Weber's law. *Phil. Trans. R. Soc. Lond. B* **366**, 3049–3057 (2011).
17. Boubenec, Y., Shulz, D.E. & Debregeas, G. Whisker encoding of mechanical events during active tactile exploration. *Front. Behav. Neurosci.* **6**, 74 (2012).
18. Knutsen, P.M., Derdikman, D. & Ahissar, E. Tracking whisker and head movements in unrestrained behaving rodents. *J. Neurophysiol.* **93**, 2294–2301 (2005).
19. Pearson, M.J., Mitchinson, B., Sullivan, J.C., Pipe, A.G. & Prescott, T.J. Biomimetic vibrissal sensing for robots. *Phil. Trans. R. Soc. Lond. B* **366**, 3085–3096 (2011).
20. Prescott, T.J., Pearson, M.J., Mitchinson, B., Sullivan, J.C.W. & Pipe, A.G. Whisking with robots. *IEEE Robot. Autom. Mag.* **16**, 42–50 (2009).
21. Towal, R.B., Quist, B.W., Gopal, V., Solomon, J.H. & Hartmann, M.J. The morphology of the rat vibrissal array: a model for quantifying spatiotemporal patterns of whisker-object contact. *PLoS Comput. Biol.* **7**, e1001120 (2011).
22. Pfeifer, R. & Gomez, G. Morphological computation: connecting brain, body and environment. in *Creating Brain-like Intelligence: From Basic Principles to Complex Intelligent Systems* (eds. Sendhoff, B., Körner, E., Sporns, O., Ritter, H. & Doya, K.) 66–83 (2009).
23. Knutsen, P.M., Pietr, M. & Ahissar, E. Haptic object localization in the vibrissal system: behavior and performance. *J. Neurosci.* **26**, 8451–8464 (2006).
24. O'Connor, D.H. *et al.* Vibrissa-based object localization in head-fixed mice. *J. Neurosci.* **30**, 1947–1967 (2010).
25. Deutsch, D., Pietr, M., Knutsen, P.M., Ahissar, E. & Schneidman, E. Fast feedback in active sensing: touch-induced changes to whisker-object interaction. *PLoS ONE* **7**, e44272 (2012).
26. Mitchinson, B., Martin, C.J., Grant, R.A. & Prescott, T.J. Feedback control in active sensing: rat exploratory whisking is modulated by environmental contact. *Proc. Biol. Sci.* **274**, 1035–1041 (2007).
27. O'Regan, J.K. & Noe, A. A sensorimotor account of vision and visual consciousness. *Behav. Brain Sci.* **24**, 939–973, discussion 973–1031 (2001).
28. Euler, L. *Enestrom Number 65: Methodus Inveniendi Lineas Curvas Maximi Minimive Proprietate Gaudentes, Sive Solutio Problematis Isoperimetrici Lattissimo Sensu Accepti* (Marcum-Michaelem Bousquet and Socios, Geneva, 1744).
29. Hill, D.N., Curtis, J.C., Moore, J.D. & Kleinfeld, D. Primary motor cortex reports efferent control of vibrissa motion on multiple timescales. *Neuron* **72**, 344–356 (2011).
30. Gordon, G. & Ahissar, E. Hierarchical curiosity loops and active sensing. *Neural Netw.* **32**, 119–129 (2012).
31. Ahissar, E., Abeles, M., Ahissar, M., Haidarliu, S. & Vaadia, E. Hebbian-like functional plasticity in the auditory cortex of the behaving monkey. *Neuropharmacology* **37**, 633–655 (1998).
32. Ego-Stengel, V., Shulz, D.E., Haidarliu, S., Sosnik, R. & Ahissar, E. Acetylcholine-dependent induction and expression of functional plasticity in the barrel cortex of the adult rat. *J. Neurophysiol.* **86**, 422–437 (2001).
33. Bahar, A., Dudai, Y. & Ahissar, E. Neural signature of taste familiarity in the gustatory cortex of the freely behaving rat. *J. Neurophysiol.* **92**, 3298–3308 (2004).
34. Saig, A., Gordon, G., Assa, E., Arieli, A. & Ahissar, E. Motor-sensory confluence in tactile perception. *J. Neurosci.* **32**, 14022–14032 (2012).
35. Ahissar, E. & Knutsen, P.M. Object localization with whiskers. *Biol. Cybern.* **98**, 449–458 (2008).
36. Horev, G. *et al.* Motor-sensory convergence in object localization: a comparative study in rats and humans. *Phil. Trans. R. Soc. Lond. B* **366**, 3070–3076 (2011).
37. Mitchinson, B. *et al.* Empirically inspired simulated electro-mechanical model of the rat mystacial follicle-sinus complex. *Proc. Biol. Sci.* **271**, 2509–2516 (2004).
38. Lottem, E. & Azouz, R. A unifying framework underlying mechanotransduction in the somatosensory system. *J. Neurosci.* **31**, 8520–8532 (2011).
39. Hill, D.N., Bermejo, R., Zeigler, H.P. & Kleinfeld, D. Biomechanics of the vibrissa motor plant in rat: rhythmic whisking consists of triphasic neuromuscular activity. *J. Neurosci.* **28**, 3438–3455 (2008).

40. Simony, E. *et al*. Temporal and spatial characteristics of vibrissa responses to motor commands. *J. Neurosci.* **30**, 8935–8952 (2010).
41. Haidarliu, S., Simony, E., Golomb, D. & Ahissar, E. Muscle architecture in the mystacial pad of the rat. *Anat. Rec.* (*Hoboken*) **293**, 1192–1206 (2010).
42. Stüttgen, M.C., Kullmann, S. & Schwarz, C. Responses of rat trigeminal ganglion neurons to longitudinal whisker stimulation. *J. Neurophysiol.* **100**, 1879–1884 (2008).
43. Pammer, L. *et al*. The mechanical variables underlying object localization along the axis of the whisker. *J. Neurosci.* (in the press) (2013).
44. O'Connor, D.H., Peron, S.P., Huber, D. & Svoboda, K. Neural activity in barrel cortex underlying vibrissa-based object localization in mice. *Neuron* **67**, 1048–1061 (2010).
45. Knutsen, P.M., Biess, A. & Ahissar, E. Vibrissal kinematics in 3D: tight coupling of azimuth, elevation, and torsion across different whisking modes. *Neuron* **59**, 35–42 (2008).
46. Sachdev, R.N., Sato, T. & Ebner, F.F. Divergent movement of adjacent whiskers. *J. Neurophysiol.* **87**, 1440–1448 (2002).
47. Chiel, H.J., Ting, L.H., Ekeberg, Ö. & Hartmann, M.J.Z. The brain in its body: motor control and sensing in a biomechanical context. *J. Neurosci.* **29**, 12807–12814 (2009).
48. Cramer, N.P. & Keller, A. Cortical control of a whisking central pattern generator. *J. Neurophysiol.* **96**, 209–217 (2006).
49. Harish, O. & Golomb, D. Control of the firing patterns of vibrissa motoneurons by modulatory and phasic synaptic inputs: a modeling study. *J. Neurophysiol.* **103**, 2684–2699 (2010).
50. Herfst, L.J. & Brecht, M. Whisker movements evoked by stimulation of single motor neurons in the facial nucleus of the rat. *J. Neurophysiol.* **99**, 2821–2832 (2008).

ONLINE METHODS

Animal maintenance and all experimental procedures were conducted in accordance with the guidelines of the US National Institutes of Health and the Weizmann Institute of Science.

Animals. Male albino Wistar rats ($n = 58$, 180–330 g, 2–3.5 months old) were held 1–4 in a cage in a 12-h dark/light cycle and were studied in three settings during both dark and light periods of their cycle: 45 under anesthesia using artificial whisking, 7 under a head fixation procedure and 6 during an object localization task. Sample sizes were determined by statistical requirements.

Artificial whisking under anesthesia. Artificial whisking was induced by stimulating the buccal motor branch of the facial nerve under urethane anesthesia as described previously[7,8]. Between 0 (typically) and 5 whiskers were trimmed in each experiment to increase video quality or simplify object positioning. With artificial whisking, a small stimulus-locked component (83 Hz in our case) was superimposed on the main protraction trajectory[7].

Head-fixed awake rats. Prior to the experiments, rats were fitted with head posts for head fixation under ketamine and xylazine anesthesia, as previously described[25,45,51]. All whiskers were trimmed, except for three whiskers (C1, C2 and D1) on each side of the snout[25]. The maximal time for head fixation was 30 min. Head fixation was terminated earlier if rats showed signs of distress. A vertical metal pole (2.8 mm in diameter), attached to a micrometer-resolution linear actuator (Abiry), was moved along the anterior-to-posterior axis on either the right or left side of the snout at an average velocity of 1.1 cm s^{-1}. The pole trajectory constrained the range of radial distances of the majority of contacts to 8–16 mm (**Fig. 6c**).

Freely moving rats during object localization. Rats were trained to palpate two stationary vertical poles, presented at both sides of the snout, and report the side in which the pole was located more posterior, as described previously[23]. Briefly, the azimuthal offset between the two vertical poles varied between trials according to a staircase procedure, whereby task difficulty increased after correct trials and decreased after incorrect trials. The maximum azimuthal offset was 20 mm. The lower limit of presented offsets was determined by the performance of the rats. Correct trials were rewarded with a drop of fruit juice. When particular performance criteria were reached, whiskers were trimmed down to a single row, single arc or single whisker on each side of the snout. The object angle (**Fig. 4h**) was the angle subtended between the caudo-rostral axis of the head and a line drawn between the base of the contacting whisker and the object.

Imaging follicle movements under anesthesia. Follicles were exposed by straight, 5–7-mm-long incisions into the skin of the whisker pad between two neighboring rows of whiskers. After incising the skin, the connective tissues surrounding the upper and most outer part of the follicle were carefully separated to ensure that no internal muscles surrounding the follicle were damaged. High-magnification, high-speed video images of the follicle were taken at 500 fps with a high-speed digital video camera (MotionScope PCI 1000, Redlake) fitted with a bright optics macro lens (105 mm, $f = 2.8$).

Tracking and analysis of whisker movements. In anesthetized rats ($n = 45$ rats), movement trajectories of 39 whiskers were analyzed; of these, 27 were tested in all 3 radial positions, 31 in all 3 azimuthal positions and 19 in all 6 azimuthal-radial positions. In head-fixed rats ($n = 7$ rats), 3,011 whisking cycles of 7 whiskers were recorded, out of which 1,992 randomly selected cycles were analyzed. In freely moving rats, 109 whisking cycles in rats having all whiskers intact ($n = 3$ rats) and 2,956 whisking cycles of 6 whiskers in rats performing the task with a single whisker on each side of the snout ($n = 3$ rats) were analyzed.

Whiskers were from rows A through E and columns 0 (straddlers) through 4. Whisker movements were recorded at 500 or 1,000 fps with fast digital video cameras (MotionScope PCI and MotionPro series, resolutions 320 × 280 to 1,280 × 512 pixels, Redlake). Movements of full-length whiskers were video tracked in all frames with a semi-automated program written in MATLAB and C[18] (freely available at http://code.google.com/p/whiskertracker/). In brief, for every whisker appearing in the video, we fitted a three-point piecewise polynomial (spline); in some cases a five-point spline was fitted (see below). The mechanical parameters of the whiskers were calculated from the spline as follows. The whisker angle was computed at its base (being the most proximal point of the tracked whisker) from the coefficients of the most proximal polynomial of the whisker-spline representation

$$\theta = \arctan\left(f'|_{x=0}\right) = \arctan(C)$$

for the polynomial $f(x) = Ax^3 + Bx^2 + Cx + D$, where x is the radial coordinate and $x = 0$ is the whisker base. We computed curvature from the coefficients of the same polynomial

$$\kappa = \left.\frac{f''}{(1+f'^2)^{1.5}}\right|_{x=0} = \frac{2B}{(1+C^2)^{1.5}} \quad (2)$$

using the standard formula for curvature of a one-dimensional function at a point[52] (see below). Curvature can be also expressed as the inverse of the radius of the whisker-spline osculating circle, that is, the circle that shares the same tangent as the whisker-spline at the measurement point (**Fig. 1e**; also see ref. 52).

$$|\kappa| = \frac{1}{r}$$

Thus, the smaller the radius of an osculating circle, the larger the curvature, and a straight whisker with no curvature would have an osculating circle with a radius equal to infinity.

Angle absorption (θ_a) was defined as the difference between the actual angle during touch and the angle at a corresponding phase of the cycle during whisking in free air (**Fig. 1i**)

$$\theta_a = \theta_{\text{free air}} - \theta_{\text{touch}} \quad (3)$$

Angle protraction (θ_p) was defined as the difference between the angle of the whisker and its value at touch onset

$$\theta_p = \theta_{\text{touch}} - \theta_{\text{touch onset}} \quad (4)$$

Velocity change following contact ($\Delta\omega$) was defined as the mean velocity of the whisker between the moment of touch onset (contact, t_c) and $t_c + 10$ ms, relative to the velocity during the same period measured under free air conditions

$$\Delta\omega = [\omega(t_c)_{\text{free air}} - \omega(t_c)_{\text{touch}}]/\omega(t_c)_{\text{free air}} \quad (5)$$

where

$$\omega(t_c)_{\text{free air}} = [\theta_{\text{free air}}(t_c + \Delta T) - \theta_{\text{free air}}(t_c)] / \Delta T$$

$$\omega(t_c)_{\text{touch}} = [\theta_{\text{touch}}(t_c + \Delta T) - \theta_{\text{touch}}(t_c)] / \Delta T$$

ΔT was arbitrarily set at 10 ms, as, during active touch, touch-contact cells of the trigeminal ganglion respond to touch within 10 ms[7].

Curvature analysis: global, at base and along the whisker shaft. Global curvature ($G\kappa$) was the maximal curvature (κ, equation (2)) along a cubic spline function fitted to a substantial part of the bending portion of the whisker, taken here to be the portion between its base and the point of contact with the object (**Fig. 5b**). Base curvature ($B\kappa$) was evaluated by fitting a cubic spline function to a small portion of the whisker close to its base and calculating κ at the point closest to the base (**Fig. 5a**). Local curvature along the whisker shaft was evaluated in high-resolution images by fitting a five-point spline function to the entire whisker and calculating κ for each point along the whisker shaft. The average local curvature for each point was calculated by sliding a window of 50 pixels (~2 mm) along the reproduced whisker shaft. This analysis was done for each object position, at maximum whisker protraction. $G\kappa_p$ ($B\kappa_p$) was quantified as the maximal difference between $G\kappa$ ($B\kappa$) during touch and $G\kappa$ ($B\kappa$) following touch onset.

Statistical analysis. ANOVA tests were one way with repeated measures (variances had similar magnitudes; we considered whiskers to be independent whether or not they came from the same rat). Non-parametric Kolmogorov-Smirnov tests were two sample and two sided. Data are expressed as mean ± s.e.m. Pole

position in anesthetized rats and pole side in head-fixed rats were randomized using a uniform distribution. Pole offset polarity in freely moving rats was pseudo-randomized by a bias-correcting rule[23]. No blinding was done during analysis and none of the data points were excluded.

51. Pietr, M.D., Knutsen, P.M., Shore, D.I., Ahissar, E. & Vogel, Z. Cannabinoids reveal separate controls for whisking amplitude and timing in rats. *J. Neurophysiol.* **104**, 2532–2542 (2010).
52. Weisstein, J.S., Goldsby, R.E. & O'Donnell, R.J. Oncologic approaches to pediatric limb preservation. *J. Am. Acad. Orthop. Surg.* **13**, 544–554 (2005).

doi:10.1038/nn.3378